*Smart Structures and Systems, Vol. 3, No. 2 (2007) 201-217* 
DOI: http://dx.doi.org/10.12989/sss.2007.3.2.201

# Active damage localization technique based on energy propagation of Lamb waves

Lei Wang† and F. G. Yuan‡

*Department of Mechanical and Aerospace Engineering, North Carolina State University, Campus box 7921, Raleigh, NC 27695-7921, USA*

*(Received March 31, 2006, Accepted December 19, 2006)*

**Abstract.** An active damage detection technique is introduced to locate damage in an isotropic plate using Lamb waves. This technique uses a time-domain energy model of Lamb waves in plates that the wave amplitude inversely decays with the propagation distance along a ray direction. Accordingly the damage localization is formulated as a least-squares problem to minimize an error function between the model and the measured data. An active sensing system with integrated actuators/sensors is controlled to excite/receive $A_0$ mode of Lamb waves in the plate. Scattered wave signals from the damage can be obtained by subtracting the baseline signal of the undamaged plate from the recorded signal of the damaged plate. In the experimental study, after collecting the scattered wave signals, a discrete wavelet transform (DWT) is employed to extract the first scattered wave pack from the damage, then an iterative method is derived to solve the least-squares problem for locating the damage. Since this method does not rely on time-of-flight but wave energy measurement, it is more robust, reliable, and noise-tolerant. Both numerical and experimental examples are performed to verify the efficiency and accuracy of the method, and the results demonstrate that the estimated damage position stably converges to the targeted damage.

**Keywords:** damage localization; least-squares method; structural health monitoring; Lamb waves; wavelet transform; wave energy.

---

## 1. Introduction

In the future, aerospace vehicles will be designed with integrated health monitoring systems that will monitor critical structural components. Conventional non-destructive evaluation (NDE) techniques can not be directly applied to monitor the structural health since these techniques usually rely on in-laboratory testing and require bulky instruments (Thomas 1995). Especially for these vehicles, the structural health monitoring (SHM) system is required to perform on *in situ* structures with minimum manual interference. Therefore, integrated monitoring components such as sensors, either surface-mounted or embedded in the structures, are compulsory in these circumstances (Boller and Biemans 1997). Various methods to monitor the structural health have been proposed in the past decade (Doebling, *et al.* 1996, Housner, *et al.* 1997, Chang 1999, Sohn, *et al.* 2003). SHM technology has been integrated on DC-XA Delta Clipper to demonstrate in-flight health monitoring (Huang 2001). The demonstrated SHM technologies include passive acoustic emission flight system and sensors, and fiber/

---

†Ph.D. candidate, E-mail:wangleibox@hotmail.com
‡Professor, Corresponding author, E-mail: yuan@ncsu.edu

optic/conventional sensors on its composite liquid hydrogen tank and critical structures. The acoustic emission technology will be demonstrated on the X-34 primary structure during flight for SHM. Besides sensors, actuators exciting diagnostic signals can also be surface-mounted on or embedded in the structures to build an active SHM system. Major advantages of an active SHM system over a passive one (without built-in actuators) include higher repeatability, accuracy, and reliability of assessing the structural integrity from the collected sensor data, because the active SHM is subjected to prescribed actuation. In contrast, the acoustic signature in passive acoustic emission approaches is unique to the damage and is only emitted once.

Several methods based on acoustic emission technique and wave propagation have been investigated for impact source localization. Tobias (1976) presented a triangulation method to detect a single damage in a plate with three sensors. He approached the problem as three interesting circles; each centered at a sensor, with their radii determined the time difference of arrival (TDOA) of the wave pack from the source to the respective sensor. Jeong and Jang (2000) proposed another triangulation method, in which the TDOA between two sensors was evaluated first, and then the damage was located at the crossing point of two hyperbolas. However, two common features of these methods need to be noticed. First, the triangulation methods are well suited in the wave-based acoustic emission where the strain energy is suddenly released by the initiation or extension of the damage and is carried by elastic waves. Thus, using acoustic emission sensors to detect the location is passive sensing, not active detection. Second, these two methods need to evaluate the TDOA of the response waves. Due to the ambiguity of arrival time or time-of-flight and the signals often contaminated with environmental and service-related noise, the measurement of TDOA may not be accurate enough to be determined and incurs errors in predicting the damage location. For active damage detection, Wang, *et al*. (2001) developed an active diagnostic system to identify damage in composite and concrete materials with four surface-mounted PZT sensors. This system employed an optimization algorithm to locate the damage center and evaluate the dimension of the damage, but the measurements were based on arrival times of damage scattering waves and each sensor needed to play both actuator and sensor roles alternately. Although Kehlenbach and Hanselka (2003) introduced an active damage localization technique by using four PZT sensors and scattered Lamb waves from damage, the time-of-flight was still needed to be evaluated in advance and at least two of these sensors had to act as actuator and sensor alternately. Recently Sohn, *et al*. (2004) developed an active sensing system to effectively identify composite delamination, which was based on continuous wavelet transform and signal attenuation rather than time-of-flight. The method had a relatively low monitored-area-to-sensor-number ratio: 61 cm × 61 cm area needed 16 sensors.

In this paper, an energy model of Lamb wave propagating in plates is first introduced. Then a least-squares method is applied to iteratively searching an incipient damage location based on energy measurements of $A_0$ mode of Lamb waves. The proposed method possesses several advantages over other triangulation methods. First the method achieves active damage detection which is suitable for the application of SHM. Second the signals collected by sensors are used in the algorithm without measuring the time-of-flight or TDOA which is oftentimes ambiguous to be measured. Third the proposed method has relatively high monitored-area-to-sensor-number ratio: 60×60 cm$^2$ area only needs 4 sensors. Lastly, environmental noise can be readily taken into account in the model. An active sensing system is set up to validate the feasibility of the least-squares damage localization method. From the simulated and experimental results on an aluminum plate, it is shown that the estimated damage position makes good agreement with the targeted damage location.

## 2. Wave energy decay model of Lamb waves

In wave analysis of isotropic plates, Yang and Yuan (2005) have recently developed asymptotic solutions of flexural waves using Mindlin plate theory. Applying the stationary phase method, the asymptotic solutions of transverse deformation and slope of a transverse normal at the midplane of the plate for long times $t$ and propagation distances $r$ with $r/t$ held fixed can be expressed as

$$w(r, t) \sim \sqrt{\frac{2\pi}{rt}} \sum_{\substack{stationary \\ points\ k}} \frac{F_1(k)}{\sqrt{\omega''(k)}} \exp i\left[kx - \omega(k)t - \frac{\pi}{4}\operatorname{sgn}\omega''(k)\right] \tag{1}$$

$$\psi(r, t) \sim \sqrt{\frac{2\pi}{rt}} \sum_{\substack{stationary \\ points\ k}} \frac{F_2(k)}{\sqrt{\omega''(k)}} \exp i\left[kx - \omega(k)t - \frac{\pi}{4}\operatorname{sgn}\omega''(k)\right] \tag{2}$$

where $\omega(k)$ is the dispersion relation between $\omega$ and $k$; $k=k(r,t)$ is the stationary point which is root of the equation $\omega'(k) = r/t$; $F_1(k), F_2(k)$ are associated with the initial conditions or loading. Furthermore the above equations hold for $d^2\omega/dk^2 \neq 0$ and single wave mode (Yang and Yuan 2005). Since time $t$ equals to $r/c_g$ in which $c_g$ is the group velocity, it can be concluded from Eqs. (1) and (2) that for a fixed wave frequency the wave amplitude inversely decays with propagation distance along a ray direction. Additionally, the group velocity $c_g$ is independent of wave propagation direction in isotropic plates.

Fig. 1 displays group velocity dispersion curves of antisymmetric Lamb waves $A_0$ and $A_1$ in an aluminum plate Al-6061 from both Mindlin plate theory and three-dimensional elasticity theory. Note that in the figure $f$ is the wave frequency, $h$ is the total thickness of the plate and $c_T = \sqrt{G/\rho}$ denotes

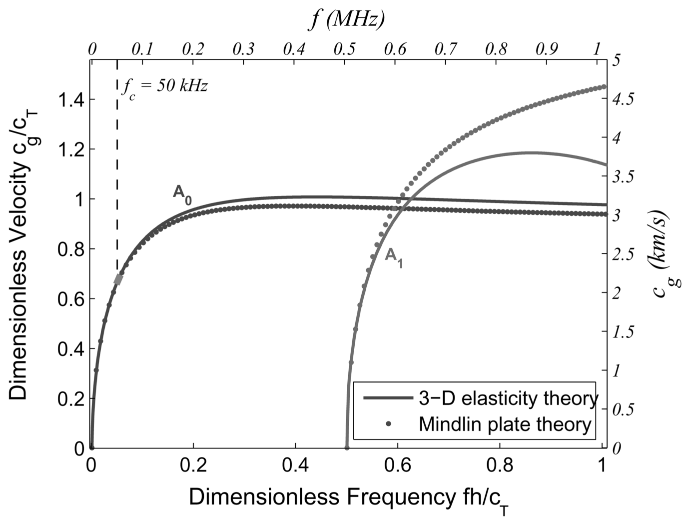


Fig. 1 Group velocity dispersion curves of antisymmetric Lamb wave from 3-D elasticity theory and Mindlin plate theory

the transverse (or shear) wave velocity in the plate, where $G$ is shear modulus. Actual and nondimensional frequency and group velocity are both shown in the figure. It may be seen that Mindlin plate theory and 3-D elasticity theory match very well over the beginning portion of each mode. In order to generate pure $A_0$ mode, the excitation frequency of actuator must be less than the first cut-off dimensionless frequency $fh/c_T = 0.5$ (or $f = 505$ kHz). Furthermore, utilizing Eqs. (1) and (2) requires $d^2\omega/dk^2 \neq 0$, that is the frequency of excitation should be away from the flat portion of the group velocity curve of $A_0$ mode shown in Fig. 1. Accordingly, in this study the excitation frequency of actuator is chosen as 50 kHz, and the corresponding group velocity $c_g$ for $A_0$ mode equals 2107 m/s. In addition when the excitation is a narrowband tone-burst wave signal and its central frequency is much less than the cut-off frequency of $A_1$, the dispersion effect is minimized and all the excited waves are dominated by the $A_0$ mode (Lin and Yuan 2001a).

In order to obtain the scattered waves solely from damage, the response wave signals are collected before and after damage occurred at each sensor. Then the pre-damage wave signals are subtracted from the post-damage wave signals. Let $M$ be the number of sensors, $N$ be the amount of sensor data collected by each sensor. Suppose $N$ is sufficiently large so that the noise can be modeled as a stationary Gaussian distribution. Fig. 2 shows the scheme of sensor and actuator deployment with the damage location. It is known from Eqs. (1) and (2) that in the low frequency range the amplitude of elastic waves in a plate decays at a rate inversely proportional to the propagation distance. Since the size of incipient damage is small and it can be treated as a secondary wave source, the time series of scattered wave signal received by each sensor can be modeled as:

$$x_m(n) = s_m(n) + \upsilon_m(n), \quad m = 1, 2, \ldots, M, \quad n = 1, 2, \ldots, N \tag{3}$$

and

$$s_m(n) = \gamma_m \frac{\alpha a_0(n - t_m - \tau)}{\|\boldsymbol{\rho} - \mathbf{r}_m\|} \tag{4}$$

where $x_m(n)$: the $n$th value sampled at the $m$th sensor over time interval $1/f_s$;

$f_s$: sampling rate;

$\upsilon_m(n)$: zero-mean additive white Gaussian noise of sensor $m$ with variance $\sigma_m^2$;

$\gamma_m$: sensor gain factor of the $m$th sensor;

$\boldsymbol{\rho}$ : position vector of the damage;

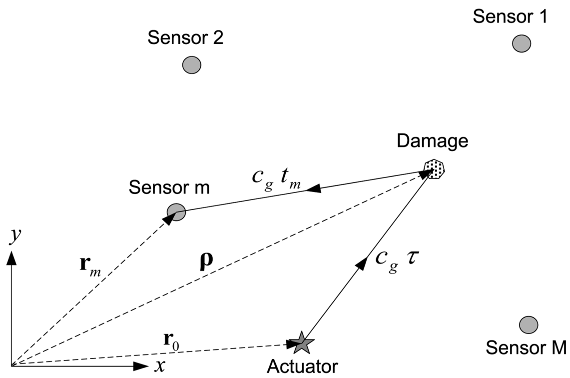


Fig. 2 Scheme of sensor/actuator deployment and unknown damage

$\mathbf{r}_m$: Cartesian coordinates of the sensor $m$;
$\alpha$ : damage scattering factor;
$a_0(n-t_m-\tau)$ : normalized scattered waveform from damage with unit peak-to-peak value;
$t_m$: time delay from the damage to sensor $m$;
$\tau$ : time delay from the actuator to the damage.

$$t_m = f_s\|\boldsymbol{\rho}-\mathbf{r}_m\|/c_g \text{ and } \tau = f_s\|\boldsymbol{\rho}-\mathbf{r}_0\|/c_g \tag{5}$$

where $\mathbf{r}_0$ is a given vector denoting Cartesian coordinates of the actuator, and the operator $\|\ \|$ indicates Euclidean distance. It is worth noting that sampling rate $f_s$ in Eq. (5) converts physical time delays (unit in second) to corresponding sampled time series.

If there is no damage in the plate, the scattered wave signal received by each sensor $x_m(n)$ is nothing but Gaussian noise. Therefore, the existence of damage can be simply determined by observing appearance of scattered wave signals.

The excitation signal is a Hanning windowed sinusoid burst signal governed by the following function:

$$q(t) = P[H(t)-H(t-N_p/f_c)]\times[1-\cos(2\pi f_c t/N_p)]\sin(2\pi f_c t) \tag{6}$$

where $H(t)$ is the Heaviside step function, $P$ is the voltage, $N_p$ is the number of peaks of the excitation and $f_c$ is the central frequency. In this study, $N_p$=5, and $f_c$=50kHz are used.

The scattered waveform is assumed to have the same shape as Eq. (6) and the mathematical expectation of $a_0(n)$, or even with time delay, equals to zeros if $N$ is large enough, since $q(t)$ is obviously a zero-mean signal.

$$E[a_0(n)] = 0, E[a_0(n-t_m-\tau)] = 0 \tag{7}$$

Assume $s_m(n)$ and $\upsilon_m(n)$ are independent and uncorrelated such that $E[s_m(n)\upsilon_m(n)] = E[s_m(n)] \cdot E[\upsilon_m(n)] = 0$, it follows from Eq. (5) that

$$E[x_m^2(n)] = E[s_m^2(n)] + E[\upsilon_m^2(n)] \tag{8}$$

The mathematical expectation of energy is calculated by averaging over a time window $T = N/f_s$. Denoting the scalar $E[x_m^2(n)]$ as $\hat{y}_m$ and knowing $E[\upsilon_m^2(n)]$ equals its variance $\sigma_m^2$, the energy decay model can be expressed as:

$$\hat{y}_m = E[x_m^2(n)] = \frac{1}{N}\sum_{n=1}^{N} x_m^2(n) = \frac{g_m}{N}\sum_{n=1}^{N}\left[\frac{\alpha a_0(n-t_m-\tau)}{\|\boldsymbol{\rho}-\mathbf{r}_m\|}\right] + \sigma_m^2 \tag{9}$$

where $g_m = \gamma_m^2$ and time series $a_0(n-t_m-\tau)$ is a $N\times 1$ vector.

In practice, $\hat{y}_m$ is the modeled wave energy which estimates the scattered wave at the $m$th sensor and the corresponding measured wave energy is $y_m$, which may be viewed as the extracted characteristic from the collected data at the $m$th sensor. $\sigma_m^2$ is the variance of background noise in sensor $m$ and can be measured. Thus, before performing any optimization algorithm, $2M$ known values $\{y_1, y_2 \ldots y_M; \sigma_1, \sigma_2, \ldots \sigma_M\}_{2M}$ need to be obtained.

In Eq. (9), we have two unknown variables of the damage location described by $\boldsymbol{\rho} = (\rho_x, \rho_y)$ and one unknown damage scattering factor $\alpha$. Totally, three unknown parameters are

$$\boldsymbol{\theta} = \{\rho_x \; \rho_y \; \alpha\}_3 \tag{10}$$

Since three unknown variables need to be estimated, there must be at least three or more sensors reporting wave energy measurements, $M \geq 3$, to yield a solution for single damage location.

## 3. Least-squares damage localization method

Mathematically, locating damage is an inverse problem. The estimated damage location can be calculated from collected signals such that the error function can reach its minimum. In the least-squares method, the unknown variables are iteratively updated to minimize the following error function:

$$J(\boldsymbol{\theta}) = \frac{1}{2}\sum_{m=1}^{M}(y_m - \hat{y}_m)^2 \tag{11}$$

where $y_m$ and $\hat{y}_m$ are the measured and modeled wave energy at sensor $m$, respectively.

The gradient of $J(\boldsymbol{\theta})$ with respect to $\alpha$ is

$$\frac{\partial J(\boldsymbol{\theta})}{\partial \alpha} = 2\alpha \sum_{m=1}^{M} g_m(y_m - \hat{y}_m)\frac{1}{N}\sum_{n=1}^{N}\frac{a_0^2(n - t_m - \tau)}{\|\boldsymbol{\rho} - \mathbf{r}_m\|^4} \tag{12}$$

The gradient of $J(\boldsymbol{\theta})$ with respect to the $p$th component of damage location $\boldsymbol{\rho}$ can be expressed as

$$\begin{aligned}\frac{\partial J(\boldsymbol{\theta})}{\partial \boldsymbol{\rho}_{.p}} = {} & 2\alpha^2 \sum_{m=1}^{M} g_m(y_m - \hat{y}_m)\frac{1}{N}\sum_{n=1}^{N}\left[\frac{(r_{m.p} - \boldsymbol{\rho}_{.p})a_0^2(n - t_m - \tau)}{\|\boldsymbol{\rho} - \mathbf{r}_m\|^4}\right. \\ & \left. + \frac{2f_s}{c_g}\frac{a_0(n - t_m - \tau)a_0'(n - t_m - \tau)}{\|\boldsymbol{\rho} - \mathbf{r}_m\|^2}\cdot\left(\frac{r_{m.p} - \boldsymbol{\rho}_{.p}}{\|\boldsymbol{\rho} - \mathbf{r}_m\|} + \frac{r_{0.p} - \boldsymbol{\rho}_{.p}}{\|\boldsymbol{\rho} - \mathbf{r}_0\|}\right)\right]\end{aligned} \tag{13}$$

where the subscript. $p$ denotes the $p$th component of coordinates ($x$ or $y$) and the prime is the derivative with respect to its argument.

Then for the next iteration the variables will be updated as

$$\alpha^{(i+1)} = \alpha^{(i)} - \varsigma_1\frac{\partial J(\boldsymbol{\theta})}{\partial \alpha} \tag{14}$$

$$\boldsymbol{\rho}_{.p}^{(i+1)} = \boldsymbol{\rho}_{.p}^{(i)} - \varsigma_2\frac{\partial J(\boldsymbol{\theta})}{\partial \boldsymbol{\rho}_{.p}} \tag{15}$$

where step sizes $\varsigma_1$ and $\varsigma_2$ are positive scalars.

The above procedure leads to a so-called Gradient optimization algorithm:

Gradient optimization algorithm
Initialization:
Initial damage positions $\{\rho\}$ and
damage scattering factors $\alpha$
Repeat until convergence
Calculate Eqs. (12) and (13)
Update Eqs. (14) and (15)
The convergence criterion is given by

$$\|\rho^{(i+1)} - \rho^{(i)}\| \le 0.0001 \tag{16}$$

## 4. Simulations and experiments

### *4.1. Simulation study*

In this section, damage localization verified by using simulated data and the proposed least-squares method is demonstrated as follows. The material properties of aluminum plate (Al-6061) are listed in Table 1. The central frequency of the excitation signal is set as 50 kHz which is much less than the cut-off frequency of $A_1$ waves such that only the lowest antisymmetric wave $A_0$ can exist. Using 3-D elasticity theory, the group velocity $c_g$ of the lowest antisymmetric wave $A_0$ can be obtained as 2107 m/s.

In order to generate the simulated wave signal received by each sensor, a finite difference algorithm based on Mindlin plate theory is used to synthesize the waves in the aluminum plate (Lin and Yuan 2001b, Wang and Yuan 2005). A 600×600 finite difference mesh with uniform square grid space $\Delta x = \Delta y = 2.54$ is superimposed on the plate region. The thickness of the plate is 0.32 cm. The origin of the coordinate system is set at the center of the plate. A single damage is located at (20,10)cm. The point damage is modeled as a material with one-sixteenth times value of the bending and transverse shear stiffness for the undamaged plate. In addition, the excitation emits at the origin and four sensors are located at (-30,30)cm, (30, -30)cm, (30, 30)cm and (-30, 30)cm to form a square region. The parameters of excitation signal in Eq. (6) are set as $N_p = 5$, and $f_c = 50\text{kHz}$. Fig. 3 displays the simulated damage scattering wave signals received at four sensors by using the finite difference algorithm. Since the plate is large enough so that there is no wave reflected from the boundary during the time span of data record. From, it may be seen that the scattered waves from the damage are still packed in the time domain under the tone-burst excitation, but the slight dispersion effect can be observed.

The additive noise of each sensor is set the same as Gaussian noise with zero-mean $\mu = 0$ and standard variance $\sigma^2 = 0.01$. Every sensor shares the same gain factor $\gamma_m = 200$. In addition, the signal-to-noise-ratio (SNR) is defined in the following to evaluate the effect of additive noise:

$$\text{SNR} = 10 \log\left(\frac{y_m - \sigma^2}{\sigma^2}\right)(\text{db}) \tag{17}$$

Fig. 4 shows the scattered wave form after adding Gaussian noise and the calculated SNR at each sensor. In order to detect the damage location at (20, 10)cm, from Section 2, the minimum number of sensor is 3. Figs. 5 and 6 show the localization results for three-sensor setup and four-sensor setup, respectively, and the searching tracks in these two figures are updated every forty steps.

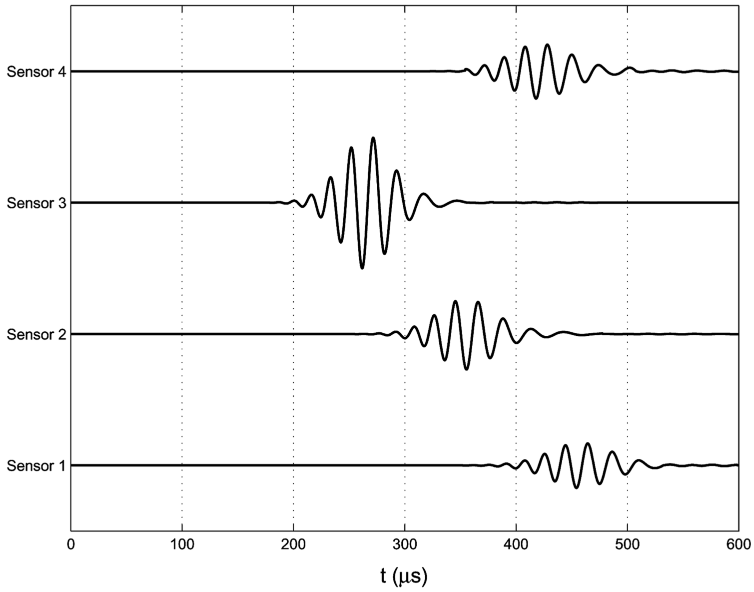


Fig. 3 Simulated scattered wave packs from the damage using finite difference method

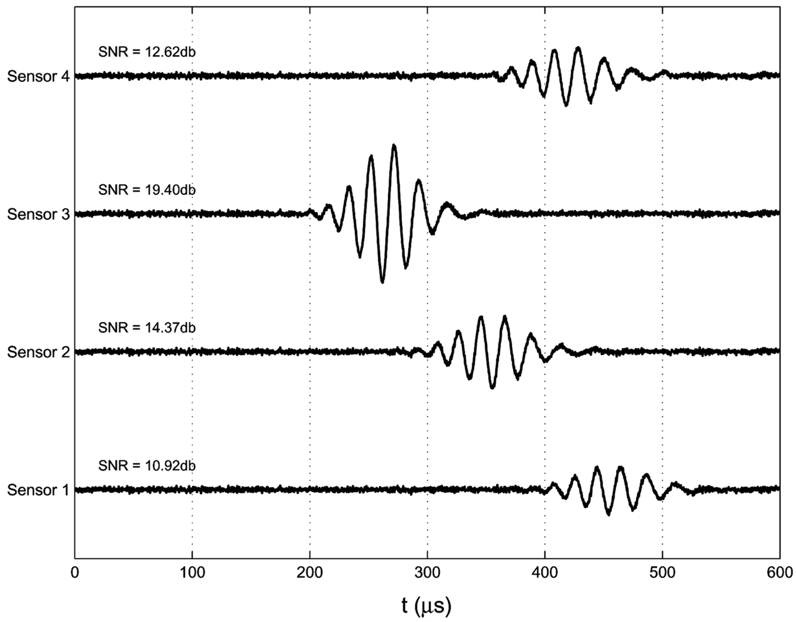


Fig. 4 Simulated scattered wave packs with the zero-mean additive Gaussian noise

The simulated sensor data from sensor 1 to sensor 3, which are shown in Fig. 4, are used for damage location with three-sensor setup. In Fig. 5, although the estimated location approaches the targeted damage location, the rate of convergence is relatively low. The error in location remains relatively high after 1400 iterations. The location error is the Euclidean distance between the targeted location and

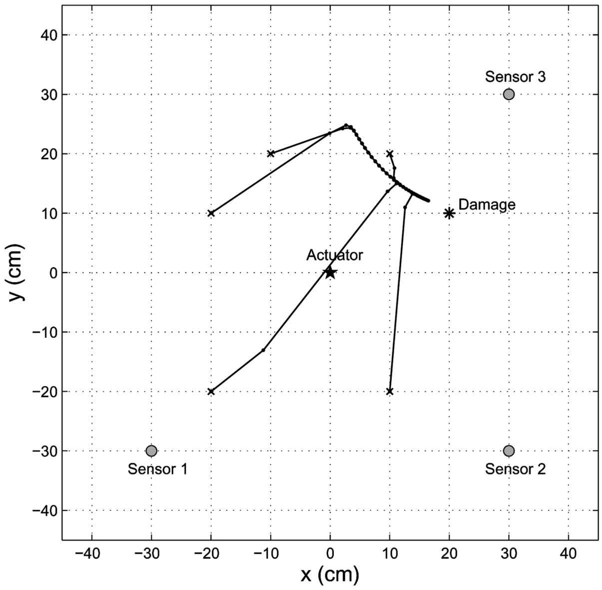


Fig. 5 Single damage localization using three sensors

estimated location. The estimated damage location is (16.7, 12.1)cm which is deviated from the targeted damage location by 3.9 cm. Comparing with distance 60 cm between sensor 1 and sensor 2, the method may be acceptable in practical applications.

Compared to three sensors case, the searching procedure is speed up remarkably when four sensors are used. After 500 iterations, the location error decreases to 1.2 cm. The estimated damage location is (18.8, 10.1)cm deviated from the targeted damage location (20, 10)cm. Thus more sensors can effectively reduce the number of iterations. On the other hand, more sensors may also increase the computational cost. There is a trade-off between the number of sensors and computational cost. Generally the former effect is dominant, thus the number of sensors should be somewhat larger than the necessary number of sensors in the application of real-time damage detection.

Figs. 5 and 6 also show the different searching tacks with different initial guess positions. It can be seen that this method has a robust performance and good convergence.

### 4.2. Experimental study

In this section, the least-squares method is performed on experimental signals to validate its capability of damage localization. An aluminum plate Al-6061 with dimension 91 cm × 91 cm × 0.32 cm is prepared and two circular rare-earth magnet stones with diameter 1.2 cm are placed on both sides of the plate at (20,10)cm to simulate a damage. Table 1 lists the material properties of the plate. A pair of PZT disks, Navy Type II PKI502 (Piezo Kinetics Inc.) are surface-mounted on both upper and lower sides at the central location of the plate, which is the origin of the coordinates, to act as an actuator and the other four pieces of PZT disks are bonded near the four corners of the plate. Note that the diameter of PZT sensor is 6.4 mm and the thickness is 1.57 mm. The experimental setup as shown in Fig. 7 consists of an Agilent 33120A function generator, K-H7602 amplifier, a Tektronix TDS 420A digital oscilloscope, and a computer connected through a GPIB interface. The Agilent 3220A function generator produces a

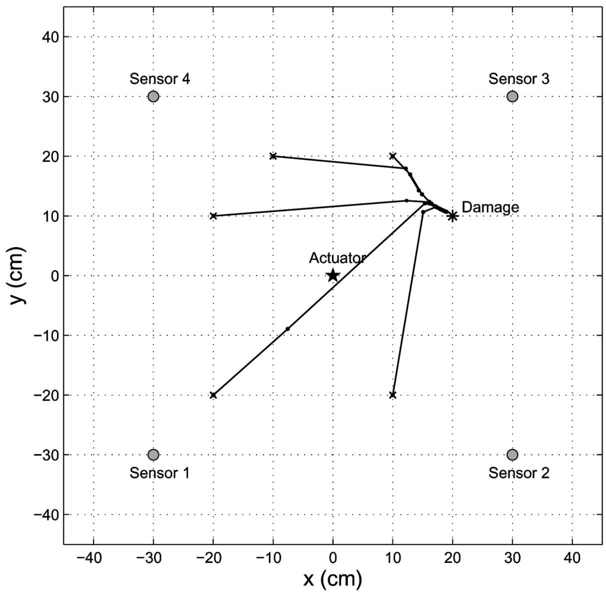


Fig. 6 Single damage localization using four sensors

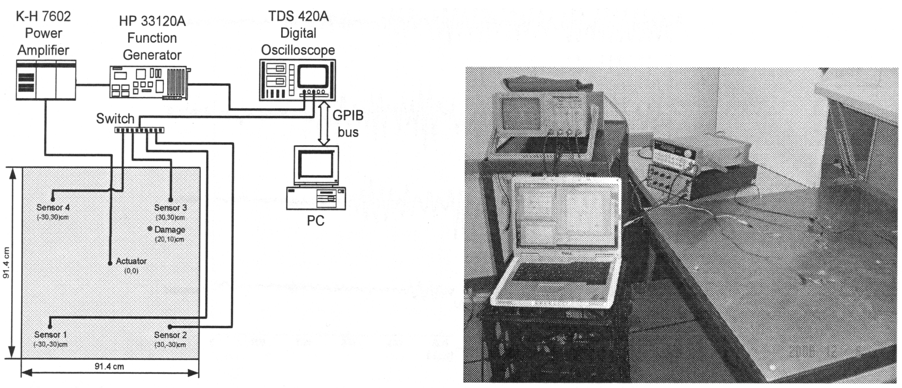


(a) Diagram (b) Actual setup

Fig. 7 Experimental setup for damage localization

Table 1 Material properties and geometry of Al-6061 plate

| $E$ (GPa) | $\nu$ | $\rho$ (kg/m$^3$) | $h$ (m) | Dimension (m×m) |
|---|---|---|---|---|
| 72.0 | 0.3 | 2730 | 0.032 | 0.91× 0.91 |

50 kHz tone-burst signal with 10 Hz repetition rate. Meanwhile, the signal is sent to the oscilloscope and through the amplifier. The sampling rate of the digital oscilloscope is set as 500 kHz. The peak voltage of the excitation signal from the amplifier is kept at ±50 V, which translates into an electric field intensity of about 31.25 V/mm, below the maximum operating field 300 V/mm of the PZT disk. Then the response signals recorded by PZT sensors are displayed and stored in the digital oscilloscope.

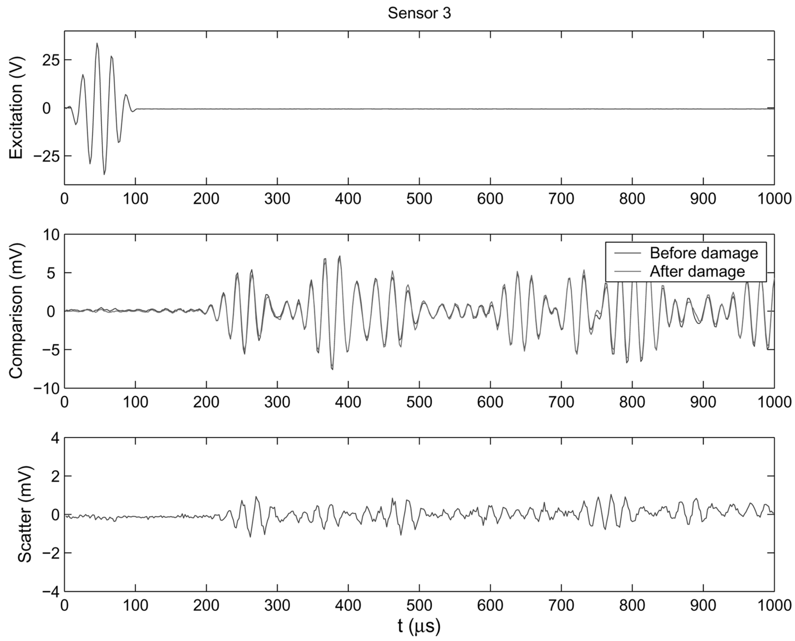


Fig. 8 Excitation signal, the response wave signals before and after damage occurred, and the scattered waves at sensor 3

Finally, computer obtains the collected sensor date via GPIB interface and runs the least-squares algorithm to estimate the damage location.

In Fig. 8, the upper plot shows the waveform of the excitation signal in time domain, the middle plot displays the response wave signals collected by sensor 3 before and after the damage occurred, and the lower plot is the scattered wave from the damage, which is obtained by subtracting the response wave signal before damage occurred from the response wave signal after damage occurred. From the scattered wave signal, the first wave pack from the damage can be clearly recognized; however, besides the first arrival pack (at 270 μs), several scattered wave packs also exist in the lower plot of Fig. 8. Since the simulated damage using magnetic stone mounted the plate, the wave packs between 300 μs and 700 μs may be the scattered waves from the boundaries of the damage; and the wave packs after 700 μs are generated from the boundary reflection of the plate. In addition, Fig. 9 shows the scattered wave signals from damage received by the four sensors. Due to different voltage scales, the signal received at sensor 3 looks much more noisy in Fig. 9 than in Fig. 8. In Fig. 9, the mean drift in time histories is incurred by power line noise (60 Hz in USA). It has been removed before executing the searching algorithm.

In order to extract the first scattered wave pack and eliminate the unwanted scattered waves, a discrete wavelet transform (DWT) (Mallat 1998) is performed before running the least-squares algorithm. Firstly, the original signal is decomposed into five levels by DWT, in which one approximation signal $a_5$ and five detail signals $d_1$~$d_5$ can be obtained. Fig. 10 shows the structure of decomposed signals and their corresponding frequency bandwidths. Since the sampling rate is 500 kHz, based on Shannon Theory (Mallat 1998, Shannon 1949) the maximum frequency $f_{\max}$ of the received signal is 250 kHz. On the other hand, the excitation signal is narrow-banded and its central frequency equals to

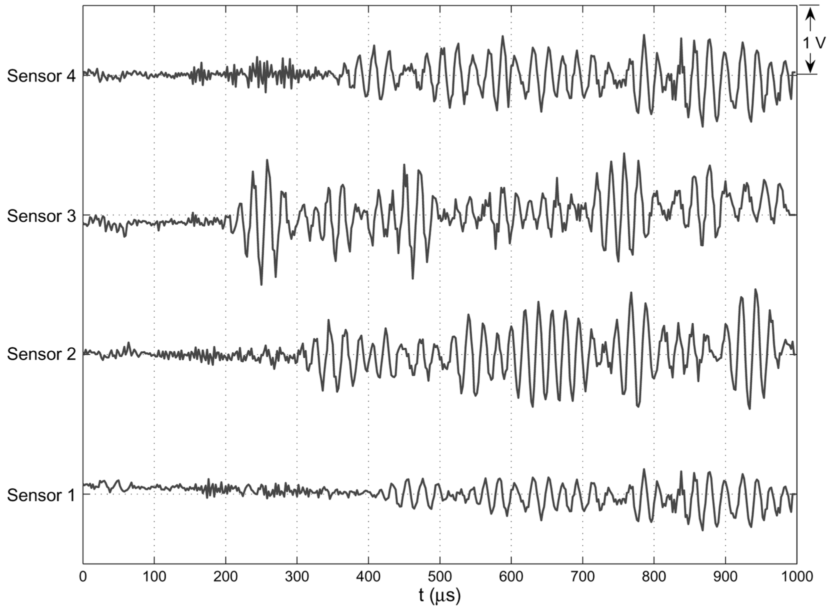


Fig. 9 Scattered wave signal received by each sensor for targeted damage at (20, 10)cm

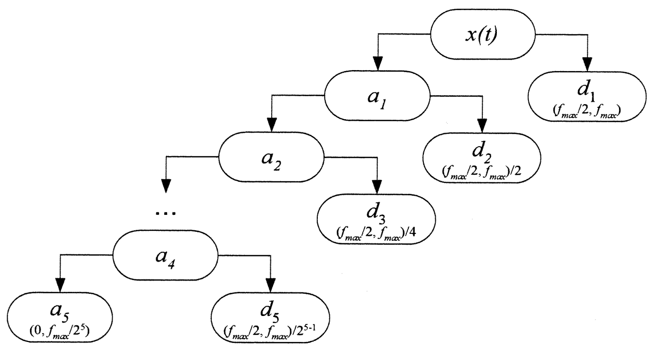


Fig. 10 Tree decomposition algorithm of DWT and bandwidth of each level

50 kHz. Thus, the bandwidth of level 3, which is (31.25, 62.5)kHz, contains 50 kHz signals, i.e., the wave energy concentrates most in this level as shown in Fig. 11. Secondly, in level 3 the portion of the signal after the first scattered wave pack is set to zero and the other portions in this level are unchanged. Additionally, the decomposed signals in the other levels remain unchanged. Thirdly, after extracting the first scattered wave pack, the wave signal can be reconstructed by using $d_1$~$d_5$ levels. Fig. 12 shows the reconstructed signals at sensor 3. Repeating this procedure for the rest of the signals, scattered wave signals from the damage can be extracted as shown in Fig. 13.

With the extracted wave signals as shown in, the least-squares method is performed on these signals and the position of damage will be estimated iteratively. Fig. 14 illustrates the experimental results of damage localization by the least-squares method, in which the different searching tacks with different initial guess positions. The estimated damage position is (18.6, 10.7)cm and the error with respect to the targeted damage location (20, 10)cm is 1.6 cm.

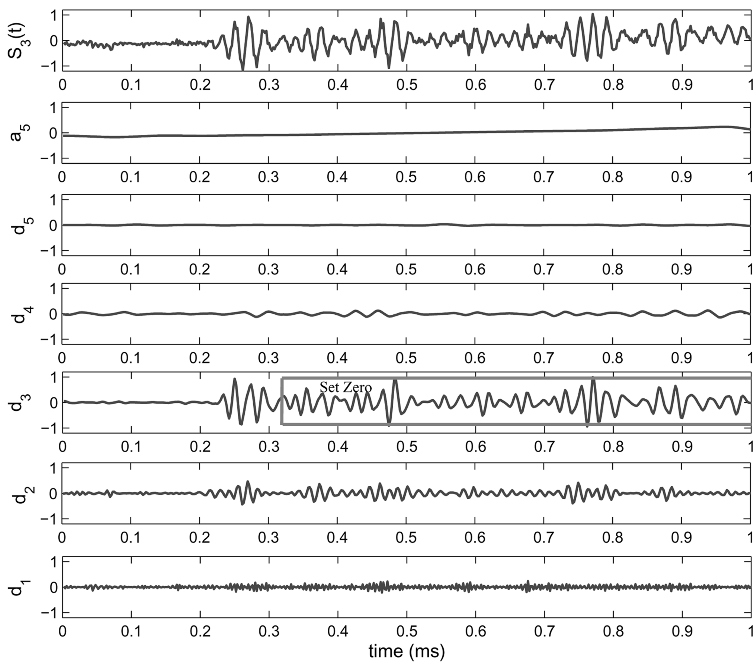


Fig. 11 Original signal at sensor 3, its decomposed signals by DWT and extraction of the first scattering at level 3

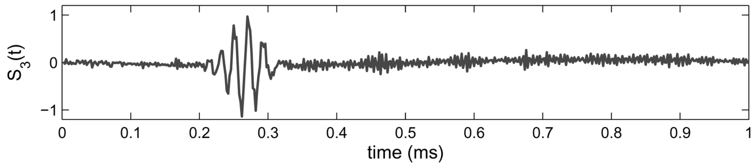


Fig. 12 Reconstructed signal at sensor 3 by using DWT and extraction of the first scattered wave signal

In order to verify the reliability of the method, the whole procedure is repeated to localize a new position of the targeted damage located at (-10, -10)cm. Fig. 15 shows the scattered wave signal from the damage received at each sensor. The final damage localization results are shown in Fig. 16, where the final estimated damage position is (-10.8, -9.39)cm and has 1.0 cm distance error with respect to the targeted damage position. Each line indicates the searching track with different initial guess positions. It can be observed from the figure that these searching tracks stably converge to a single point, thus the estimated position is independent of initial guess. According to the two damage localization examples, it may be seen that this method has a robust performance and good convergence.

## 5. Conclusions

A least-squares method is first applied to SHM field for iteratively searching a point damage location based on Lamb wave energy measurements. The proposed method has several advantages over existing triangulation methods: first the method is an active damage detection technique which is suitable for the

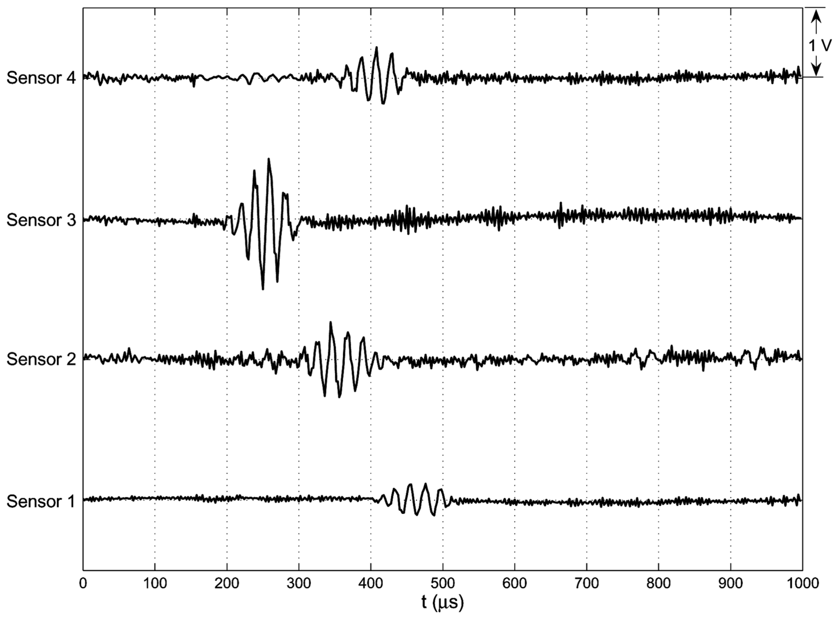


Fig. 13 Scattered wave pack directly from the damage received from each sensor after DWT

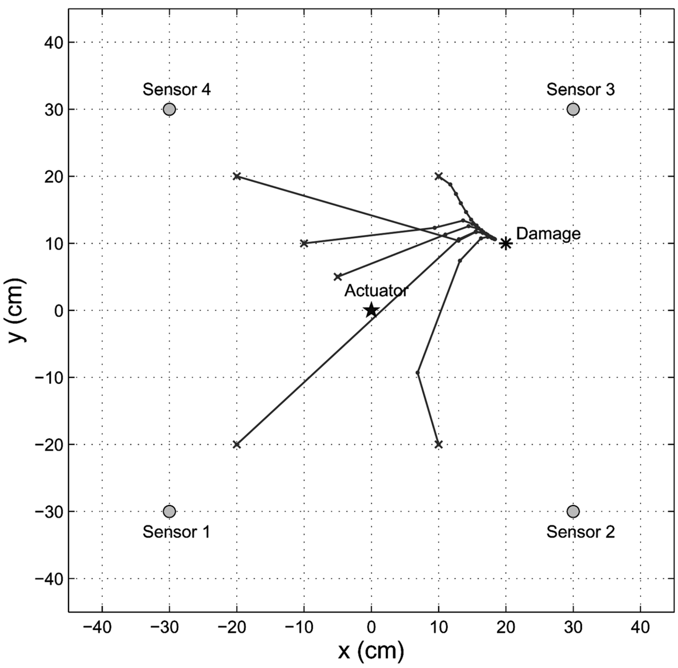


Fig. 14 Experimental result of damage localization by least-squares method for targeted damage at (20, 10) cm

application of SHM; second the method uses all the time series data information collected by each sensor without the need of measuring time-of-flight or TDOA, which is used by triangulation method; lastly the environmental noise can be taken into account. Numerical examples for damage detection are

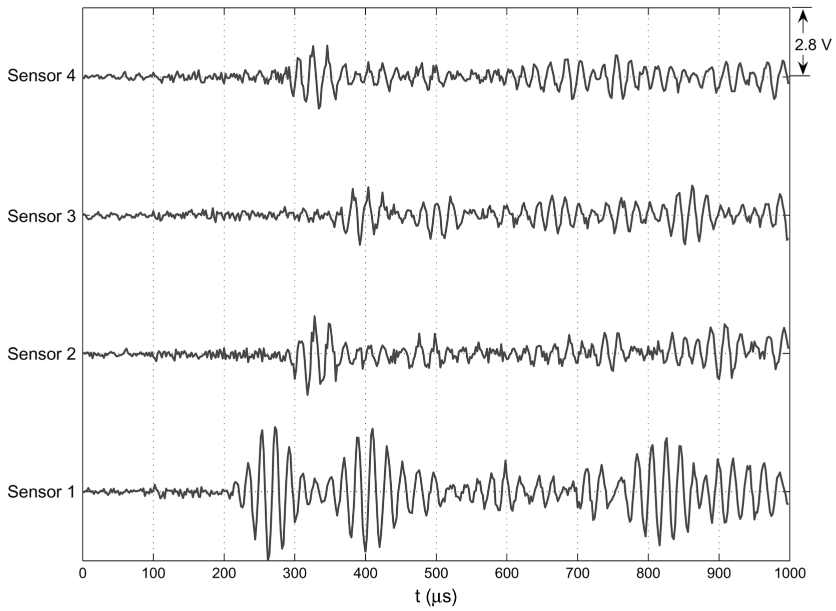


Fig. 15 Scattered wave signal received by each sensor for targeted damage at (-10, -10)cm

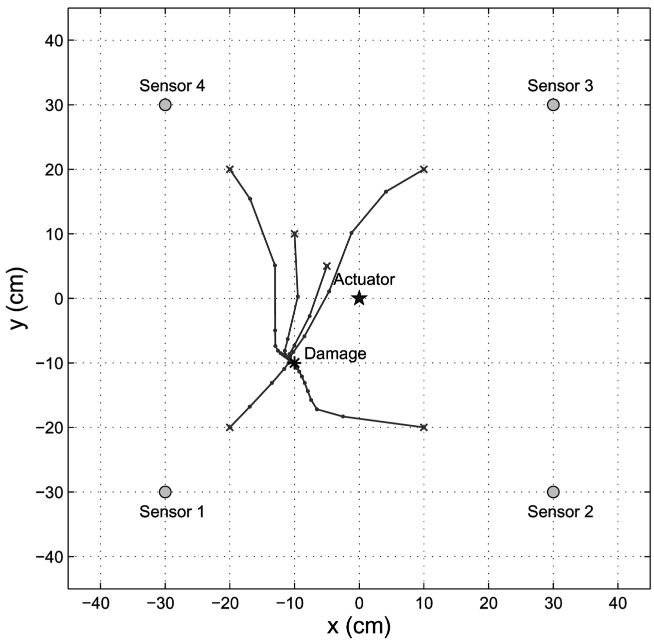


Fig. 16 Experimental result of damage localization by least-squares method for targeted damage at (-10, -10) cm

demonstrated by using the simulated sensor data computed from a finite difference algorithm. Moreover, an active sensing system is set up to validate the feasibility of the proposed method. From the simulated and experimental results, it is shown that the estimated damage location makes good agreement with the targeted location.

In the future, the entire scattered waves in original wave signal collected by each sensor need to be further investigated such that the scattered wave package from damage can be extracted automatically. For solving the non-linear least-squares equations, the gradient method employed in this study is a local minimum search method. Although the proposed method has been tested to localize multiple damages, the searched locations are much more sensitive to initial guess than single damage detection. To overcome these limitations, other advanced optimization methods, such as generic algorithm for global search, may be introduced in the future, that can be potentially used for detecting multiple damages. Furthermore, with the recent development of wireless sensor networks in SHM, the proposed least-squares method can be fused with a wireless sensor networks to achieve an active automated SHM system for actual aerospace structures.

## Acknowledgements

This research is supported by the Sensors and Sensor Networks program from the National Science Foundation (Grant No. CMS-0329878). Dr. S. C. Liu is the program manager. The financial support is gratefully acknowledged.

## References

Boller, C. and Biemans, C. (1997), "Structural health monitoring in aircraft: state-of-the-art, perspectives and benefits", *Proceedings of the 1st International Workshop on Structural Health Monitoring*, Stanford, CA, September, 541-552.

Chang, F.-K. (1999). "Structural health monitoring, a summary report on the first international workshop on structural health monitoring", *Proceedings of the 2nd International Workshop on Structural Health Monitoring*, Stanford, CA, September, xix-xxix.

Doebling, S. W., Farrar, C. R., Prime, M. B. and Shevitz, D. W. (1996), *Damage identification and health monitoring of structural and material system from changes in their vibration characteristics: a literature* review. *Technical report*. [LA-13070-MS].

Housner, G. W., Bergman, L. A., Caughey, T. K. et al. (1997), "Structural control past, present, and future", *J. Eng. Mech.*, **123**(9), 897-971.

Huang, J. Q. (2001), "Structural health monitoring for reusable launch vehicles – an integrated system and process approach", *Proceedings of the 3rd International Workshop on Structural Health Monitoring*, Stanford, CA, September, 114-122.

Jeong, H. and Jang, Y. S. (2000), "Wavelet analysis of plate wave propagation in composite laminates", *Compos. Struct.*, **49**(4), 443-450.

Kehlenbach, M. and Hanselka, H. (2003), "Automated structural integrity monitoring based on broadband Lamb wave excitation and matched filtering", *Proceedings of the 44th AIAA/ASME/ASCE/AHS/ASC Structures, Structural Dynamics, and Materials Conference*, Norfolk, VA, April, **2**,1486-1492.

Lin, X. and Yuan, F. G. (2001a), "Diagnostic Lamb waves in an integrated piezoelectric sensor/actuator plate: analytical and experimental studies", *Smart Mater. Struct.*, **10**(5), 907-913.

Lin, X. and Yuan, F. G. (2001b), "Damage detection of a plate using migration technique", *J. Intell. Mater. Syst. Struct.*, **12**(7), 469-482.

Mallat, S. (1998), *A Wavelet Tour of Signal Processing*, Academic Press, San Diego, CA.

Shannon, C. E. (1949), "Communication in the presence of noise", *Proc. Inst. Radio. Eng.*, **37**(1), 10-21.

Sohn, H., Farrar, C. R., Hemez, F. M. et al. (2003), *A Review of Structure Health Monitoring Literature: 1996-2001 Technical Report*. [LA-13976-MS].

Sohn, H., Park, G., Wait, J. R., Limback, N. P. and Farrar, C. R. (2004), "Wavelet-based active sensing for

delamination detection in composite structures", *Smart Mater. Struct*., **13**(1), 153-160.
Thomas, G. (1995), "Overview of nondestructive evaluation techniques", *Proc. SPIE*, **2455**, 5-9.
Tobias, A. (1976), "Acoustic-emission source location in two dimensions by an array of three sensors", *NDT*, **9**(1), 9-12.
Wang, C. S., Wu, F. and Chang, F.-K. (2001), "Structure health monitoring from fiber-reinforced composites to steel-reinforced concrete", *Smart Mater. Struct.*, **10**(3), 548-552.
Wang, L. and Yuan, F.G. (2005), "Damage identification in a composite plate using prestack reverse-time migration technique", *Struct. Health Monitor*, **4**(3), 195-211.
Yang, S. and Yuan, F.G. (2005), "Transient wave propagation of isotropic plates using a higher-order plate theory", *Int. J. Solids Struct.*, **42**(14), 4115-4153.

*BS*